Generation of polarized spin-triplet Cooper pairings by magnetic barriers in superconducting junctions

Shun Tamura,[1] Yukio Tanaka,[1] and Takehito Yokoyama[2]
[1]Department of Applied Physics, Nagoya University, Nagoya 464-8603, Japan
[2]Department of Physics, Tokyo Institute of Technology, Tokyo 152-8551, Japan

(Received 14 July 2022; revised 13 January 2023; accepted 18 January 2023; published 1 February 2023)

We investigate the proximity effect in an *s*-wave superconductor/ferromagnetic metal with a Rashba spin-orbit coupling/diffusive normal metal junction and an *s*-wave superconductor/noncollinear magnetic metal/diffusive normal metal junction. We show the generation of polarized spin-triplet pairings in the diffusive normal metal due to coherent spin rotation in the intermediate magnetic regions. The emergence of the spin-triplet odd-frequency Cooper pairings can generate a zero-energy peak in the quasiparticle density of states in the diffusive normal metal.

DOI: 10.1103/PhysRevB.107.054501

I. INTRODUCTION

The emergence of spin-triplet pairings in superconductor (SC)/ferromagnet junctions has received much attention [1–4]. In ferromagnet/SC junctions, polarized spin-triplet pairings can be generated due to coherent spin rotation by inhomogeneous magnetization [5,6]. The generation of the polarized spin-triplet pairing has been confirmed by observing Josephson current through strong ferromagnets [7–9]. Polarized spin-triplet pairings are an important ingredient for superconducting spintronics. For example, in current-biased ferromagnetic Josephson junctions, one can realize spin-polarized supercurrent due to the generation of polarized spin-triplet pairings [10]. Since polarized spin-triplet pairings have a spin polarization, they can also be used to exert spin transfer torques and induce magnetization dynamics [11–15].

Even in uniform ferromagnets, polarized spin-triplet pairings can be generated by spin-orbit coupling due to coherent spin rotation [16–19]. The interplay between spin-orbit coupling and superconductivity leads to various phenomena such as a zero-energy peak in the density of states [20,21], ϕ_0 junctions [22–24], magnetoelectric effects [25,26], and enhanced spin pumping [27].

Spin-triplet pairings are also generated with the use of ferromagnetic insulators. They are generated from spin-flip scattering by inserting a ferromagnetic insulator at the interface between a normal metal and an SC [28–30] or by placing an SC on the ferromagnet insulator EuS [31–33]. Although this spin-flip scattering by homogeneous ferromagnets generates spin-triplet pairings, a Cooper pair amplitude does not have polarized spin-triplet components: the Cooper pair amplitude is not polarized since the d vector of the spin-triplet Cooper pair amplitude is parallel to the magnetization of the ferromagnet. Then, an inhomogeneous spin structure, including a combination of a homogeneous spin structure and a spin-dependent coupling, e.g., spin-orbit coupling, is necessary to induce polarized spin-triplet pairing. Recent experiments on superconducting tunnel junctions with magnetic insulators GdN and EuS have indicated the emergence of odd-frequency spin-triplet pairings [34,35], which manifests as a zero-energy peak in the local density of states [36–40]. Also, it has been predicted that the coupling between a magnon in a ferromagnetic insulator and Cooper pairs can lead to a magnon spin current [41] and the formation of magnon-cooparons [42].

In this paper, we extend the previous works that studied the generation of spin-triplet Cooper pairings in superconducting junctions with a uniform magnetic interface [28–30] to junctions with more complicated magnetic (spin) structures [43]. Although most of the previous studies about generating the polarized spin-triplet Cooper pair amplitude were based on bulk ferromagnet junctions, we show that it is induced only by the interface complex spin structure. Here, we emphasize that the interface considered in Refs. [28–30] is a homogeneous ferromagnet or magnetic impurity, and spin-triplet Cooper pairs are not polarized in these junctions. Also, we utilize a tight-binding model in which we can choose an arbitrary value of the exchange field beyond the quasiclassical theory of superconductivity, where the magnitude of the exchange field is restricted to the order of the SC gap function. We consider two kinds of junctions: an *s*-wave SC/ferromagnet with a Rashba spin-orbit coupling (RSOC)/diffusive normal metal (DN) junction and an *s*-wave SC/noncollinear magnet/DN junction. We clarify the generation of polarized spin-triplet pairings in the DN due to coherent spin rotation in the magnetic regions. The emergence of these odd-frequency spin-triplet pairings manifests as a zero-energy peak in the local density of states.

The organization of this paper is as follows. In Sec. II, we explain our model and the method of theoretical calculations. We show the numerically calculated results in Sec. III. We summarize our results in Sec. IV.

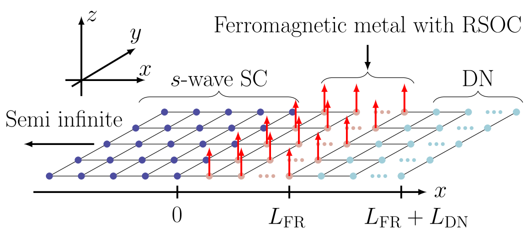

FIG. 1. Schematic picture of the s-wave SC/FR/DN junction. RSOC denotes Rashba spin-orbit coupling. We impose the periodic boundary condition in the y direction. In the negative x direction, the SC is semi-infinite, and for the positive x direction, we impose the open boundary condition at $j_x = L_{\rm FR} + L_{\rm DN}$.

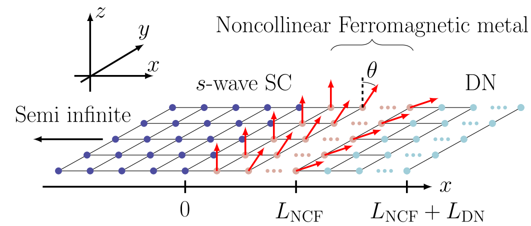

FIG. 2. Schematic picture of the s-wave SC/NCF/DN junction.

II. MODEL AND METHOD

We consider two systems: the spin-singlet s-wave SC/ferromagnetic metal with Rashba spin-orbit coupling (FR)/DN junction (Sec. II A) and the spin-singlet s-wave SC/noncollinear ferromagnetic metal (NCF)/DN junction (Sec. II B).

A. SC/FR/DN junction

The Hamiltonian for the two-dimensional SC/FR/DN junction on a two-dimensional square lattice (Fig. 1) is

$$H_l = H_t + H_{\rm SC} + H_{\rm FR} + H_{{\rm DN},l}^{L_{\rm NCF}}, \quad (1)$$

$$H_t = -t \sum_{\langle \mathbf{i},\mathbf{j}\rangle, i_x, j_x \leqslant L_{\rm FR}+L_{\rm DN}, \sigma} (c^\dagger_{\mathbf{i},\sigma} c_{\mathbf{j},\sigma} + {\rm H.c.}), \quad (2)$$

$$H_{\rm SC} = -\mu_{\rm SC} \sum_{j_x \leqslant 0, j_y, \sigma} n_{\mathbf{j},\sigma} + \Delta \sum_{j_x \leqslant 0, j_y} (c^\dagger_{\mathbf{j},\uparrow} c^\dagger_{\mathbf{j},\downarrow} + {\rm H.c.}), \quad (3)$$

$$\begin{aligned} H_{\rm FR} = & \sum_{1\leqslant j_x \leqslant L_{\rm FR}, j_y, \alpha, \beta} [h(\hat{\sigma}_z)_{\alpha,\beta} - \mu_{\rm FR}(\hat{\sigma}_0)_{\alpha,\beta}] c^\dagger_{\mathbf{j},\alpha} c_{\mathbf{j},\beta} \\ & + i\lambda \sum_{1\leqslant j_x < L_{\rm FR}, j_y, \alpha, \beta} [c^\dagger_{\mathbf{j},\alpha} (\hat{\sigma}_y)_{\alpha,\beta} c_{\mathbf{j}+\mathbf{e}_x,\beta} - {\rm H.c.}] \\ & + \lambda \sum_{1\leqslant j_x \leqslant L_{\rm FR}, j_y, \alpha, \beta} [c^\dagger_{\mathbf{j},\alpha} (\hat{\sigma}_x)_{\alpha,\beta} c_{\mathbf{j}+\mathbf{e}_y,\beta} + {\rm H.c.}], \end{aligned} \quad (4)$$

$$H_{{\rm DN},l}^{L_{\rm FR}} = \sum_{L_{\rm FR} < j_x \leqslant L_{\rm FR}+L_{\rm DN}, j_y, \sigma} (V_{\mathbf{j},l} - \mu_{\rm DN}) n_{\mathbf{j},\sigma}, \quad (5)$$

with $n_{\mathbf{j},\sigma} = c^\dagger_{\mathbf{j},\sigma} c_{\mathbf{j},\sigma}$. Here, $c_{\mathbf{j},\sigma}$ ($c^\dagger_{\mathbf{j},\sigma}$) is an annihilation (creation) operator on the $\mathbf{j}$th site with spin σ, t is a hopping integral, $\mu_{\rm SC}$ is a chemical potential in the s-wave SC region, Δ is an s-wave pair potential, h is an exchange field, $\mu_{\rm FR}$ is a chemical potential in the FR region, λ is a Rashba spin-orbit coupling, $V_{\mathbf{j},l}$ is an impurity potential in the DN region, $\mu_{\rm DN}$ is a chemical potential in the DN region, and $\hat{\sigma}_{0,x,y,z}$ is a Pauli matrix in the spin space. We use a lattice constant as a unit of length, $\langle \mathbf{i},\mathbf{j}\rangle$ in Eq. (2) denotes the sum of nearest-neighbor pairs, and $\mathbf{e}_{x(y)}$ denotes the unit vector in the x (y) direction. As a random potential $V_{\mathbf{j},l}$, we use a uniformly distributed random number ranging from $-t$ to t for each $\mathbf{j}$ and l [44,45]. The index l denotes the lth impurity sample. To calculate physical quantities, we averaged over the impurity samples from $l = 1$ to $l = N_{\rm sample}$. We impose the periodic boundary condition in the y direction with L_y sites and the open boundary condition at $j_x = L_{\rm FR} + L_{\rm DN}$ in the x direction.

Here, we consider two-dimensional systems since the computational cost of the impurity sample average is too high for more than two-dimensional systems. We expect that the qualitative results do not change: we can obtain a polarized spin-triplet Cooper pair for three-dimensional systems. It is noted that for three-dimensional systems, the spin-orbit coupling is not necessarily of the Rashba type, but it can be isotropic spin-orbit coupling.

B. SC/NCF/DN junction

The Hamiltonian for the two-dimensional SC/NCF/DN junction (Fig. 2) is

$$H_l = H_t + H_{\rm SC} + H_{\rm NCF} + H_{{\rm DN},l}^{L_{\rm NCF}}, \quad (6)$$

with

$$H_{\rm NCF} = \sum_{1\leqslant j_x \leqslant L_{\rm NCF}, j_y, \alpha, \beta} (\hat{h}_{j_x} - \mu_{\rm NCF}\hat{\sigma}_0)_{\alpha,\beta} c^\dagger_{\mathbf{j},\alpha} c_{\mathbf{j},\beta}, \quad (7)$$

$$\hat{h}_{j_x} = h[\hat{\sigma}_x \sin(j_x - 1)\theta + \hat{\sigma}_z \cos(j_x - 1)\theta]. \quad (8)$$

Here, $H_{{\rm DN},l}^{L_{\rm NCF}}$ in Eq. (6) is given by Eq. (5) by replacing $L_{\rm FR}$ by $L_{\rm NCF}$. The schematic picture of the direction of the magnetic field is shown in Fig. 2. We also impose the periodic boundary condition in the y direction with L_y sites and the open boundary condition at $j_x = L_{\rm NCF} + L_{\rm DN}$ in the x direction.

In the following, we set $\mu_{\rm SC} = \mu_{\rm FR} = \mu_{\rm NCF} = \mu_{\rm DN} = -t$ [46], $\Delta/t = 0.1$, $L_{\rm FR} = L_{\rm NCF} = 5$, and $L_{\rm DN} = 50$.

C. Local density of states and Cooper pair amplitude

In order to clarify the emergence of spin-triplet pairings and their manifestation, we calculate the local density of states (LDOS) and the anomalous Green's function. We mainly focus on the physical quantities at the center of the DN: $j_x = L_{\rm FR} + L_{\rm DN}/2$ for the SC/FR/DN junction and $j_x = L_{\rm NCF} + L_{\rm DN}/2$ for the SC/NCF/DN junction.

The Green's functions $\hat{G}_l(\tilde{z})$ of the systems are defined as

$$\hat{G}_l(\tilde{z}) = (\tilde{z} - H_l)^{-1}, \quad (9)$$

with $\tilde{z} = E + i\eta$ (positive infinitesimal η) for the retarded Green's function and $\tilde{z} = i\omega_n$ for the Green's function with Matsubara frequency [$\omega_n = (2n+1)\pi/\beta$ with inverse temperature β and $n \in \mathbb{Z}$] representation. Here, the index l stands for the lth impurity sample. The Green's functions are calculated by using the recursive Green's function method [47]. The LDOS is obtained from the normal part of the Green's function:

$$\rho_{\mathbf{j}}(E) = -\frac{1}{N_{\rm sample}\pi}\sum_{l=1}^{N_{\rm sample}} {\rm Im Tr}[PG_{l,\mathbf{j},\mathbf{j}}(E+i\eta)], \quad (10)$$

with $\eta/t = 10^{-3}$,

$$\hat{G}_l(\tilde{z}) = \begin{pmatrix} G_l(\tilde{z}) & F_l(\tilde{z}) \\ \tilde{F}_l(\tilde{z}) & \tilde{G}_l(\tilde{z}) \end{pmatrix}, \quad (11)$$

and the $\mathbf{j}$th lattice site. Here, P is a projection on the particle space: $P = (\hat{\tau}_0 + \hat{\tau}_z)/2$ with a Pauli matrix $\hat{\tau}_{0,x,y,z}$ in the particle-hole space. We discuss the average value of the LDOS in the y direction

$$\bar{\rho}_{j_x}(E) = \frac{1}{L_y}\sum_{j_y=1}^{L_y} \rho_{\mathbf{j}}(E). \quad (12)$$

In Sec. III, we show the LDOS normalized by the zero-energy LDOS for a normal metal (N)/FR/DN or an N/NCF/DN junction. Here, the Hamiltonian for the normal metal is H_l with $\Delta = 0$, and the other parameters are the same as the parameters for SC/FR/DN and SC/NCF/DN junctions, respectively. We denote the LDOS for the N/FR/DN or the N/NCF/DN junction as $\bar{\rho}_{j_x,{\rm N}}(E)$.

The Cooper pair amplitude is given by the anomalous (off-diagonal) components of the Green's function $F_l(\tilde{z})$ and $\tilde{F}_l(\tilde{z})$. Here, we focus on the component $F_l(\tilde{z})$, which has space and spin degrees of freedom:

$$F_{l,\mathbf{j},\mathbf{j}'}(\tilde{z}) = \begin{pmatrix} F_{l,\uparrow\uparrow}(\tilde{z}) & F_{l,\uparrow\downarrow}(\tilde{z}) \\ F_{l,\downarrow\uparrow}(\tilde{z}) & F_{l,\downarrow\downarrow}(\tilde{z}) \end{pmatrix}_{\mathbf{j},\mathbf{j}'}$$

$$= \sum_{\alpha=0,x,y,z} f_{l,\alpha,\mathbf{j},\mathbf{j}'}(\tilde{z})\hat{\sigma}_\alpha(i\hat{\sigma}_y) \quad (13)$$

$$= \begin{pmatrix} -f_{l,x}(\tilde{z}) + if_{l,y}(\tilde{z}) & f_{l,0}(\tilde{z}) + f_{l,z}(\tilde{z}) \\ -f_{l,0}(\tilde{z}) + f_{l,z}(\tilde{z}) & f_{l,x}(\tilde{z}) + if_{l,y}(\tilde{z}) \end{pmatrix}_{\mathbf{j},\mathbf{j}'}. \quad (14)$$

We focus on the on-site ($\mathbf{j} = \mathbf{j}'$) component expressing a local s-wave pairing since it is not affected by the impurity scattering [36,39]. We calculate the spin-triplet $\bar{F}_{j_x,{\rm t},\alpha=x,y,z}(\tilde{z})$ and the spin-singlet $\bar{F}_{j_x,{\rm s}}(\tilde{z})$ components:

$$\bar{F}_{j_x,{\rm t},\alpha}(\tilde{z}) = \frac{1}{L_y N_{\rm sample}}\sum_{l=1}^{N_{\rm sample}}\sum_{j_y=1}^{L_y} f_{l,\alpha,\mathbf{j},\mathbf{j}}(\tilde{z}), \quad (15)$$

$$\bar{F}_{j_x,{\rm s}}(\tilde{z}) = \frac{1}{L_y N_{\rm sample}}\sum_{l=1}^{N_{\rm sample}}\sum_{j_y=1}^{L_y} f_{l,0,\mathbf{j},\mathbf{j}}(\tilde{z}). \quad (16)$$

Due to the Fermi-Dirac statistics, the on-site component of the anomalous Green's function (Cooper pair amplitude) can be categorized into two types: odd-frequency spin-triplet Cooper pair amplitude [$\bar{F}_{j_x,{\rm t},\alpha}(\tilde{z}) = -\bar{F}_{j_x,{\rm t},\alpha}(-\tilde{z})$] [40,48–50] given by Eq. (15) and even-frequency spin-singlet Cooper pair amplitude [$\bar{F}_{j_x,{\rm s}}(\tilde{z}) = \bar{F}_{j_x,{\rm s}}(-\tilde{z})$] given by Eq. (16).

In the DN, anisotropic Cooper pairs, for example, the p- and d-wave Cooper pairs, are greatly suppressed due to impurity scattering irrespective of even or odd frequency, and only the s-wave pair survives. Then, we can concentrate on the s-wave Cooper pair in the DN. On the other hand, we expect that the qualitative results do not change if the DN is replaced with a ballistic metal where the polarized spin-triplet Cooper pair is also induced. We note that for a single-band case, the even-frequency s-wave Cooper pair decreases the value of the LDOS at zero energy in the DN [51,52], and the odd-frequency one increases it [36–40,53,54].

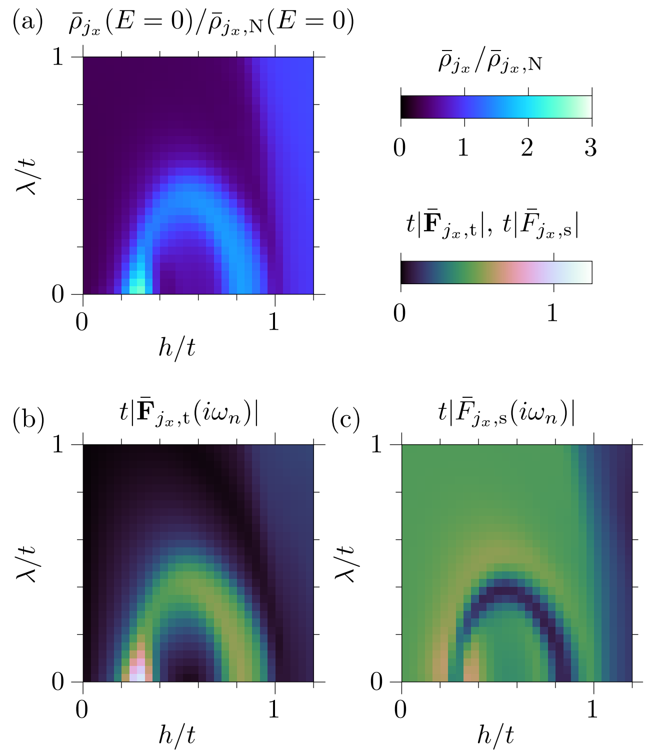

FIG. 3. (a) The normalized LDOS $\bar{\rho}_{j_x}(E=0)/\bar{\rho}_{j_x,{\rm N}}(0)$, (b) $|\bar{\mathbf{F}}_{j_x,{\rm t}}(i\omega_n)|$, and (c) $|\bar{F}_{j_x,{\rm s}}(i\omega_n)|$ are plotted as a function of h/t and λ/t at $j_x = L_{\rm FR} + L_{\rm DN}/2$. Here, $\bar{\rho}_{j_x,{\rm N}}(E)$ is the LDOS for the N/FR/DN junction. For the anomalous Green's functions, we fix $\omega_n/t = 10^{-3}$. $L_y = 100$, and $N_{\rm sample} = 10^2$ samples averaged.

Also, we calculate the following quantity [55,56]:

$$Q_{l,\alpha,\mathbf{j}}(\tilde{z}) = i[\mathbf{f}_{l,\mathbf{j},\mathbf{j}}(\tilde{z}) \times \mathbf{f}^*_{l,\mathbf{j},\mathbf{j}}(\tilde{z})]_\alpha, \quad (17)$$

with $\mathbf{f}_{l,\mathbf{j},\mathbf{j}}(\tilde{z}) = (f_{l,x,\mathbf{j},\mathbf{j}}(\tilde{z}), f_{l,y,\mathbf{j},\mathbf{j}}(\tilde{z}), f_{l,z,\mathbf{j},\mathbf{j}}(\tilde{z}))$. $Q_{l,\alpha,\mathbf{j}}(\tilde{z})$ ($\alpha = x, y, z$) is, by definition, a real quantity and expresses the polarized spin-triplet component of the Cooper pair amplitude:

$$Q_{l,z,\mathbf{j}}(\tilde{z}) = -\tfrac{1}{2}[|F_{l,\uparrow\uparrow,\mathbf{j},\mathbf{j}}(\tilde{z})|^2 - |F_{l,\downarrow\downarrow,\mathbf{j},\mathbf{j}}(\tilde{z})|^2]. \quad (18)$$

We discuss the average value of $\mathbf{Q}_{l,\mathbf{j}}(\tilde{z}) = (Q_{l,x,\mathbf{j}}(\tilde{z}), Q_{l,y,\mathbf{j}}(\tilde{z}), Q_{l,z,\mathbf{j}}(\tilde{z}))$:

$$\bar{\mathbf{Q}}_{j_x}(\tilde{z}) = \frac{1}{L_y N_{\rm sample}}\sum_{l=1}^{N_{\rm sample}}\sum_{j_y=1}^{L_y} \mathbf{Q}_{l,\mathbf{j}}(\tilde{z}). \quad (19)$$

From the definition of $Q_{l,\alpha,\mathbf{j}}(\tilde{z})$ [Eq. (17)], $Q_{l,\alpha,\mathbf{j}}(\tilde{z})$ is the product of two odd-frequency spin-triplet Cooper pair amplitudes. Then, $Q_{l,\alpha,\mathbf{j}}(\tilde{z})$ is an even function of frequency $\tilde{z}$. Here, we emphasize that we use the terminology "polarized" spin-triplet Cooper pair for $\bar{\mathbf{Q}}_{j_x}(\tilde{z}) \neq \mathbf{0}$.

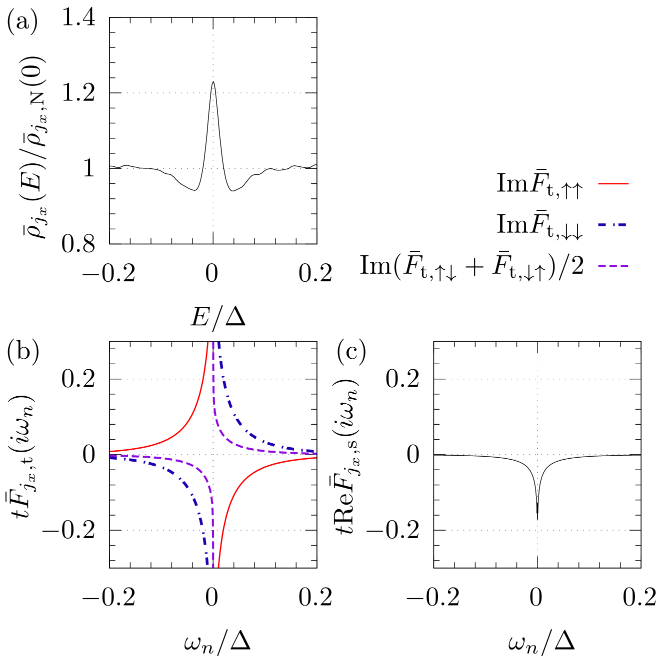

FIG. 4. (a) The normalized LDOS is plotted as a function of E. (b) $\mathrm{Im}\bar{F}_{j_x,\mathrm{t}}(i\omega_n)$ is shown as a function of ω_n. (c) $\mathrm{Re}\bar{F}_{j_x,\mathrm{s}}(i\omega_n)$ is shown as a function of ω_n. $\mathrm{Re}\bar{F}_{j_x,\mathrm{t},\uparrow\uparrow}(i\omega_n) = \mathrm{Re}\bar{F}_{j_x,\mathrm{t},\downarrow\downarrow}(i\omega_n) = \frac{1}{2}\mathrm{Re}[\bar{F}_{j_x,\mathrm{t},\uparrow\downarrow}(i\omega_n) + \bar{F}_{j_x,\mathrm{t},\downarrow\uparrow}(i\omega_n)] = \mathrm{Im}\bar{F}_{j_x,\mathrm{s}}(i\omega_n) = 0$ within numerical accuracy. $(\lambda/t, h/t) = (0.4, 0.5)$, and $j_x = L_{\mathrm{FR}} + L_{\mathrm{DN}}/2$ for (a)–(c). $L_y = 100$, and $N_{\mathrm{sample}} = 10^2$ samples averaged.

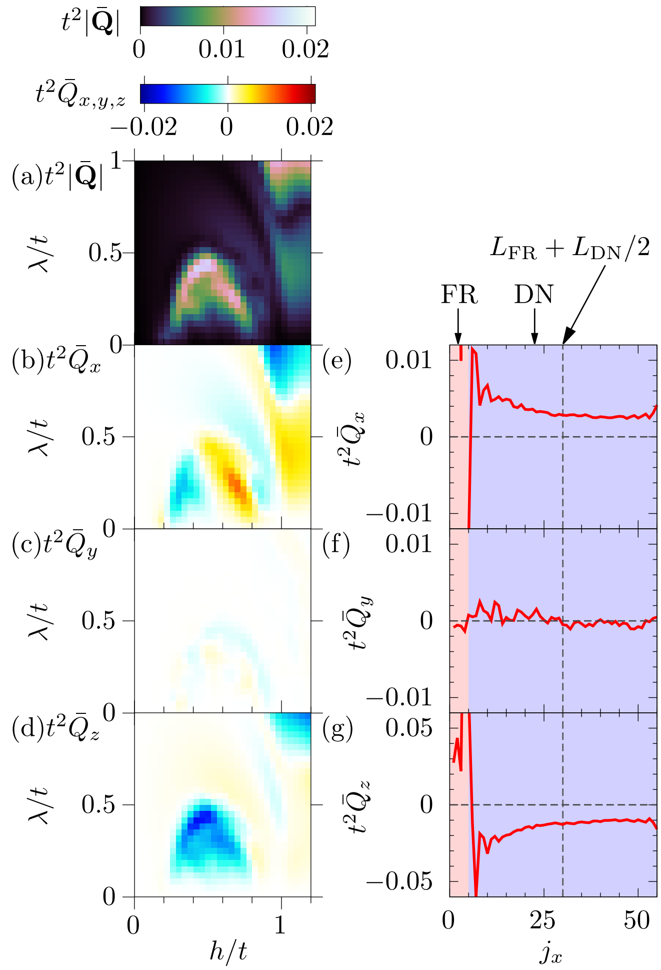

FIG. 5. (a) $|\bar{\mathbf{Q}}_{j_x}(i\omega_n)|$, (b) $\bar{Q}_{j_x,x}(i\omega_n)$, (c) $\bar{Q}_{j_x,y}(i\omega_n)$, and (d) $\bar{Q}_{j_x,z}(i\omega_n)$ are plotted as a function of h and λ at $j_x = L_{\mathrm{FR}} + L_{\mathrm{DN}}/2$. (e) $\bar{Q}_{j_x,x}(i\omega_n)$, (f) $\bar{Q}_{j_x,y}(i\omega_n)$, and (g) $\bar{Q}_{j_x,z}(i\omega_n)$ are plotted as a function of j_x at $(\lambda/t, h/t) = (0.4, 0.5)$. $j_x \in [1, 5]$ denotes the position in the FR and, $j_x \in [6, 55]$ denotes the position in the DN. $L_y = 100$, and $N_{\mathrm{sample}} = 10^3$ samples averaged.

III. RESULTS

In this section, we discuss the LDOS [Eq. (10)], the anomalous Green's functions [Eqs. (15) and (16)], and $\bar{\mathbf{Q}}_{j_x}(i\omega_n)$ [Eq. (19)]. The results for the SC/FR/DN junction are shown in Sec. III A, and those for the SC/NCF/DN junction are shown in Sec. III B. In both junctions, we obtained the polarized spin-triplet Cooper pair amplitude in the DN due to coherent spin rotation of Cooper pairs in the FR or NCF region.

A. SC/FR/DN junction

In this section, we consider the system shown in Fig. 1. In Fig. 3, we show several quantities at the center of the DN: $j_x = L_{\mathrm{FR}} + L_{\mathrm{DN}}/2$. In Fig. 3(a), the LDOS normalized by its normal state value is shown as a function of h and λ. The normalized LDOS exceeds unity due to the presence of the odd-frequency spin-triplet pairings [38–40,53,54]. It is noted that the s-wave SC junction considered in this paper is topologically trivial, and Majorana fermions never appear at the interface. Then this enhancement of the LDOS at zero energy is not related to the presence of the Majorana fermion. The normalized LDOS is the largest at approximately $(\lambda/t, h/t) = (0, 0.3)$. In Fig. 3(b), the absolute value of the spin-triplet component $|\bar{\mathbf{F}}_{j_x,\mathrm{t}}(i\omega_n)| = \sqrt{\sum_{\alpha=x,y,z} |\bar{F}_{j_x,\mathrm{t},\alpha}(i\omega_n)|^2}$, with $\omega_n/t = 10^{-3}$, is shown. Qualitatively, $|\bar{\mathbf{F}}_{j_x,\mathrm{t}}(i\omega_n)|$ at a low frequency is very similar to the LDOS: the spin-triplet Cooper pair amplitude is generated when there is a zero-energy peak in the LDOS [36–40,53,54]. In Fig. 3(c), the absolute value of the spin-singlet component $|\bar{F}_{j_x,\mathrm{s}}(i\omega_n)|$ with $\omega_n/t = 10^{-3}$ is shown. $|\bar{F}_{j_x,\mathrm{s}}(i\omega_n)|$ has a small value where the zero-energy LDOS has a large value.

In Fig. 4(a), the energy dependence of the normalized LDOS is shown for $(\lambda/t, h/t) = (0.4, 0.5)$, where the normalized LDOS is larger than unity at zero energy. We can see that there is a zero-energy peak, and corresponding to this zero-energy state, the spin-triplet component of the anomalous Green's function is largely enhanced toward zero frequency [Fig. 4(b)]. The absolute value of the spin-singlet component of the anomalous Green's function also increases for low frequency, but it approaches a finite value [Fig. 4(c)]. We also calculate the normalized LDOS and the anomalous Green's function at $(\lambda/t, h/t) = (0.8, 0.5)$, where we observe a gap-like structure in the normalized LDOS (see Appendix A).

In Fig. 5, we show $\bar{\mathbf{Q}}_{j_x}(i\omega_n)$, which reflects the polarized spin-triplet Cooper pair amplitude. In Fig. 5(a), we show $|\bar{\mathbf{Q}}_{j_x}(i\omega_n)| = \sqrt{\sum_{\alpha=x,y,z} \bar{Q}^2_{j_x,\alpha}(i\omega_n)}$. It is zero at the $h = 0$ or

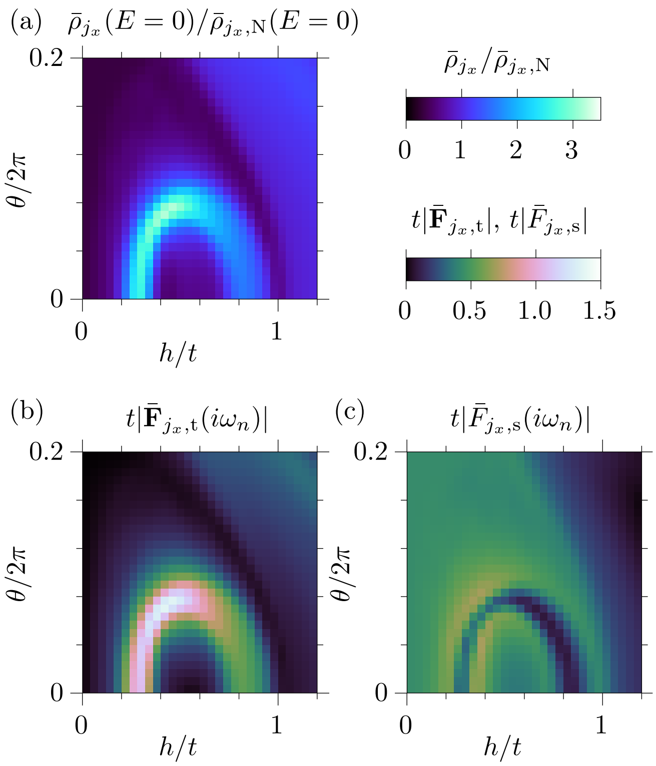

FIG. 6. (a) The normalized LDOS at zero energy, (b) $|\bar{\mathbf{F}}_{j_x,\mathrm{t}}(i\omega_n)|$, and (c) $|\bar{F}_{j_x,\mathrm{s}}(i\omega_n)|$ are plotted as a function of h and θ at $j_x = L_{\mathrm{NCF}} + L_{\mathrm{DN}}/2$. Here, $\bar{\rho}_{j_x,\mathrm{N}}(E)$ is the LDOS. For the anomalous Green's functions, we fix $\omega_n/t = 10^{-3}$. $L_y = 100$, and $N_{\mathrm{sample}} = 10^2$ samples averaged.

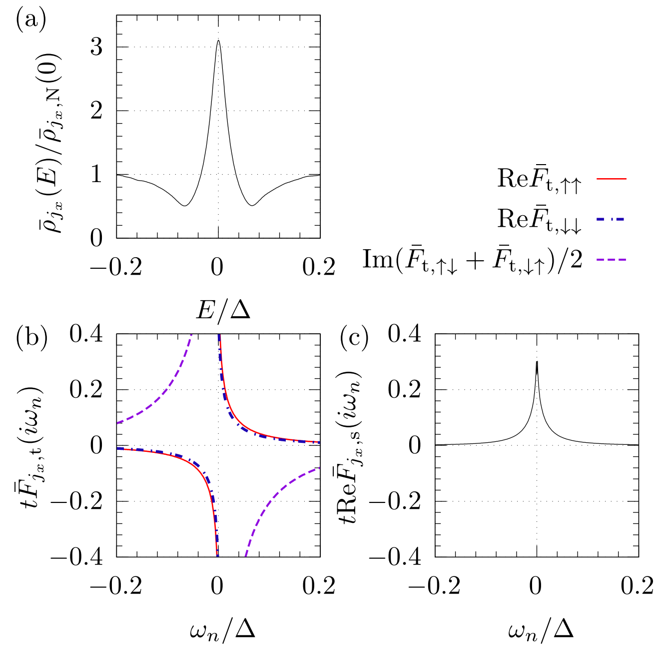

FIG. 7. (a) The normalized LDOS is plotted as a function of E. (b) $\bar{F}_{j_x,\mathrm{t}}(i\omega_n)$ is shown as a function of ω_n. (c) $\mathrm{Re}\bar{F}_{j_x,\mathrm{s}}(i\omega_n)$ is shown as a function of ω_n. $\mathrm{Im}\bar{F}_{j_x,\mathrm{t},\uparrow\uparrow}(i\omega_n) = \mathrm{Im}\bar{F}_{j_x,\mathrm{t},\downarrow\downarrow}(i\omega_n) = \mathrm{Re}[\bar{F}_{j_x,\mathrm{t},\uparrow\downarrow}(i\omega_n) + \bar{F}_{j_x,\mathrm{t},\downarrow\uparrow}(i\omega_n)] = \mathrm{Im}\bar{F}_{j_x,\mathrm{s}}(i\omega_n) = 0$ within numerical accuracy. $(\theta/2\pi, h/t) = (0, 075, 0.5)$, and $j_x = L_{\mathrm{NCF}} + L_{\mathrm{DN}}/2$ for (a)–(c). $L_y = 100$, and $N_{\mathrm{sample}} = 10^2$ samples averaged.

$\lambda = 0$ axis. This means that both h and λ must be nonzero to generate the polarized spin-triplet Cooper pairing [16,17]. We show each component of $\bar{\mathbf{Q}}_{j_x}(i\omega_n)$ as a function of h and λ in Figs. 5(b)–5(d) and their spatial dependences for $(\lambda/t, h/t) = (0.4, 0.5)$ in Figs. 5(e)–5(g). In Figs. 5(b)–5(d), all the components have nonzero values in some regions, but the y component is very small. From Figs. 5(e) and 5(g), we can see that the polarized spin-triplet Cooper pair amplitudes penetrate the DN. Also, the y component [Figs. 5(f)] has a nonzero value, but it approaches zero for a large value of the impurity sample average. The N_{sample} and L_y dependences of the normalized LDOS, $|\bar{\mathbf{F}}_{j_x,\mathrm{t}}(i\omega_n)|$, $|\bar{F}_{j_x,\mathrm{s}}(i\omega_n)|$, and $|\bar{\mathbf{Q}}_{j_x,\mathrm{t}}(i\omega_n)|$ are discussed in Sec. B 1. We discuss an expectation value of the spin operator to which the polarized spin-triplet Cooper pairs can contribute in Sec. C 1. We find that $\bar{\mathbf{Q}}_{j_x}(i\omega_n)$ and the expectation value of the spin operator are almost independent since the quasiparticles also contribute to the spin polarization.

B. SC/NCF/DN junction

Here, we show the results for the SC/NCF/DN junction. The normalized LDOS shown in Fig. 6(a) exceeds unity in some regions due to the presence of the odd-frequency spin-triplet pairings [Fig. 6(b)]. The normalized LDOS for the SC/FR/DN junction is largest when $\lambda = 0$, but for the SC/NCF/DN junction, the normalized LDOS is largest with nonzero θ. The spin-singlet Cooper pair amplitude becomes small when the spin-triplet Cooper pair amplitude has a large value [Fig. 6(c)].

In Fig. 7(a), we show the energy dependence of the normalized LDOS at $(\theta/2\pi, h/t) = (0.075, 0.5)$ and see that it has a zero-energy peak. In Figs. 7(b) and 7(c), the frequency dependences of the spin-triplet and the spin-singlet Cooper pair amplitudes are shown, respectively. The spin-triplet Cooper pair amplitude is also largely enhanced toward zero frequency, and the spin-singlet one has a nonzero value for $\omega_n \to 0$. We also show the normalized LDOS and the anomalous Green's function at $(\theta/2\pi, h/t) = (0.15, 0.5)$ in Appendix A.

The polarized spin-triplet Cooper pair amplitudes are generated in the SC/NCF/DN junction (Fig. 8). In Fig. 8(a), the absolute value of $\bar{\mathbf{Q}}_{j_x}(i\omega_n)$, with $\omega_n/t = 10^{-3}$, is shown, and it is zero for $\theta = 0$ or $h = 0$. The $h = 0$ case is trivial: there is no field, and the Hamiltonian has spin rotational symmetry. Here, the polarized spin-triplet Cooper pair amplitude has only x and z components [Figs. 8(b)–8(d)], and it might correspond to the fact that the noncollinear spin structure in the NCF lies in the x-z plane [57,58]. We also show the j_x dependence of $\bar{\mathbf{Q}}_{j_x}(i\omega_n)$ in Figs. 8(e)–8(g). Similar to the SC/FR/DN junction, the polarized spin-triplet Cooper pair amplitudes penetrate the DN. The y component of $\bar{\mathbf{Q}}_{j_x}(i\omega_n)$ is almost zero [Figs. 8(f)]. The dependences of these results on N_{sample} and L_y are discussed in Sec. B 2. We also discuss the expectation value of the spin operator in Sec. C 2, and we do not find a direct relationship between the expectation value of the spin operator and $\bar{\mathbf{Q}}_{j_x}(i\omega_n)$.

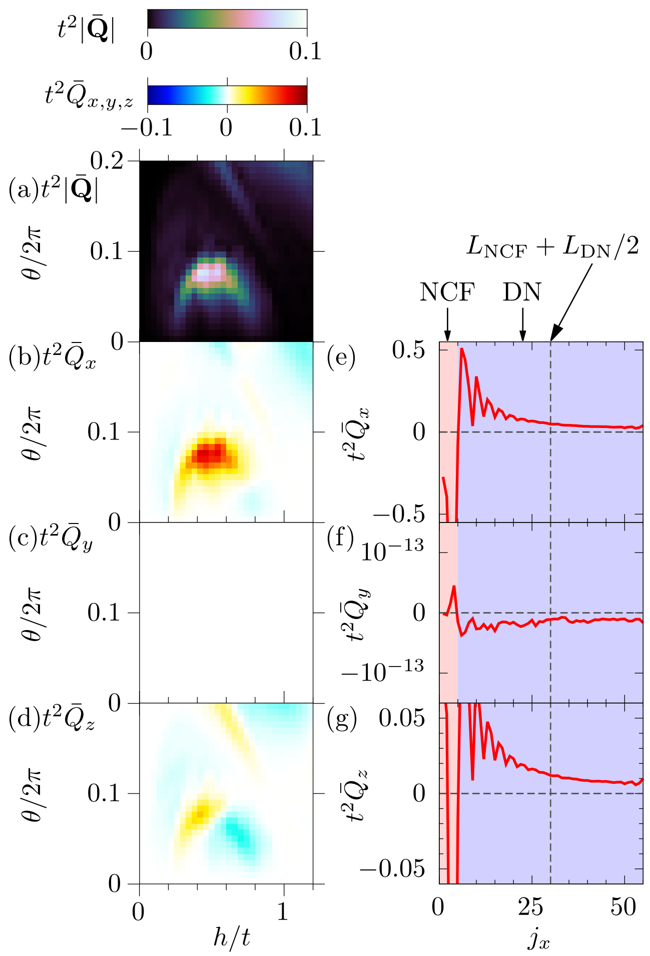

FIG. 8. (a) $|\bar{\mathbf{Q}}_{j_x}(i\omega_n)|$, (b) $\bar{Q}_{j_x,x}(i\omega_n)$, (c) $\bar{Q}_{j_x,y}(i\omega_n)$, and (d) $\bar{Q}_{j_x,z}(i\omega_n)$ are plotted as a function of h and θ for $j_x = L_{\rm NCF} + L_{\rm DN}/2$. (e) $\bar{Q}_{j_x,x}(i\omega_n)$, (f) $\bar{Q}_{j_x,y}(i\omega_n)$, and (g) $\bar{Q}_{j_x,z}(i\omega_n)$ are plotted as a function of j_x. $j_x \in [1, 5]$ is the position in the NCF, and $j_x \in [6, 55]$ is the position in the DN. In (e)–(g) $(\theta/2\pi, h/t) = (0.08, 0.5)$. $L_y = 100$, and $N_{\rm sample} = 10^3$ samples averaged.

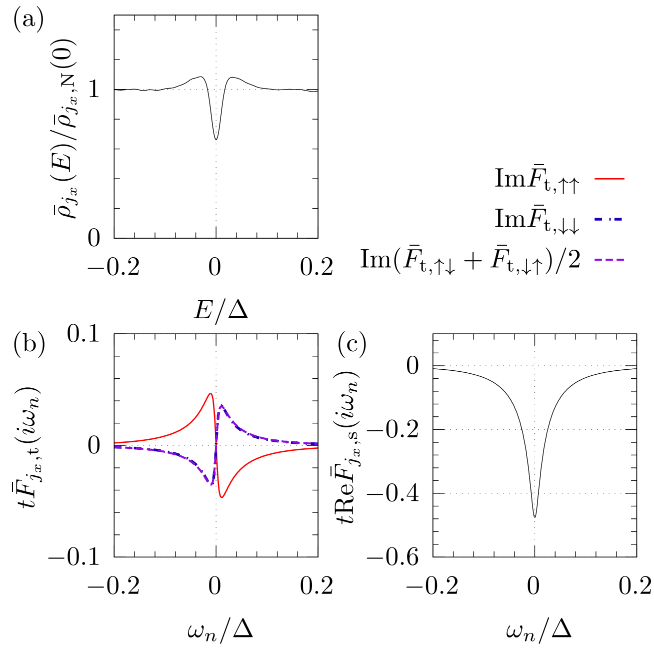

FIG. 9. (a) The normalized LDOS is plotted as a function of E. (b) $\mathrm{Im}\bar{F}_{j_x,{\rm t}}(i\omega_n)$ is shown as a function of ω_n. (c) $\mathrm{Re}\bar{F}_{j_x,{\rm s}}(i\omega_n)$ is shown as a function of ω_n. $\mathrm{Re}\bar{F}_{j_x,{\rm t},\uparrow\uparrow}(i\omega_n) = \mathrm{Re}\bar{F}_{j_x,{\rm t},\downarrow\downarrow}(i\omega_n) = \frac{1}{2}\mathrm{Re}[\bar{F}_{j_x,{\rm t},\uparrow\downarrow}(i\omega_n) + \bar{F}_{j_x,{\rm t},\downarrow\uparrow}(i\omega_n)] = \mathrm{Im}\bar{F}_{j_x,{\rm s}}(i\omega_n) = 0$ within numerical accuracy. $(\lambda/t, h/t) = (0.8, 0.5)$, $j_x = L_{\rm FR} + L_{\rm DN}/2$, $L_y = 100$, and $N_{\rm sample} = 10^2$ samples averaged.

IV. SUMMARY

In this paper, we showed that the polarized spin-triplet Cooper pair amplitude is generated by the spin-singlet s-wave superconductor in two kinds of junctions: the s-wave SC/ferromagnetic metal with Rashba spin-orbit coupling/diffusive normal metal junction and the s-wave SC/noncollinear ferromagnetic metal/diffusive normal metal junction. We have clarified the generation of the spin-polarized triplet pairings in the diffusive normal metal due to coherent spin rotation in the magnetic regions. The emergence of the triplet pairings manifests as a zero-energy peak in the density of states. Candidate magnets for these junctions are magnets without inversion symmetry [59,60] such as MnSi [61], MnGe [62], (V,Pt)Se_2 [63], and NbMnP [64]. Although we have performed numerical calculations in two-dimensional systems due to computational cost, we expect that we can obtain qualitatively the same results for three-dimensional junctions with a magnetic interface.

In this paper, we have chosen the spin-singlet s-wave pairing as the symmetry of the Cooper pair in the SC. If we choose spin-singlet d-wave pairing, zero-energy Andreev bound states [65–67] and the resulting odd-frequency pairing [40] protected by the spectral bulk-edge correspondence are generated at the interface [68]. It is an interesting issue to study the proximity effect in d-wave superconductor junctions [44] in the presence of a ferromagnetic metal with Rashba spin-orbit coupling or a noncollinear ferromagnetic metal. Also, although we concentrated on superconductor junctions with a magnetic interface as the source of the polarized spin-triplet Cooper pair in this paper, a combination of the s-wave SC and topological systems is also interesting since many topological systems require spin-orbit interaction or a magnetic field such as nanowire systems [45,69,70] and SC/topological insulator junctions [21,71–77].

ACKNOWLEDGMENTS

This work was supported by JSPS KAKENHI Grants No. JP20H00131, No. JP18H01176, No. JP20H01857, and No. JP30578216 and the JSPS-EPSRC Core-to-Core program "Oxide Superspin."

APPENDIX A: ENERGY OR FREQUENCY DEPENDENCE OF LDOS AND ANOMALOUS GREEN'S FUNCTION

In Fig. 9 (SC/FR/DN junction) and Fig. 10 (SC/NCF/DN junction), we show the energy dependence of the normalized LDOS and ω_n dependences of $\bar{\mathbf{F}}_{j_x,{\rm t}}(i\omega_n)$ and $\bar{F}_{j_x,{\rm s}}(i\omega_n)$ at the parameter where the normalized LDOS at zero energy is smaller than unity. In both graphs, we can see that there is a gaplike structure at zero energy for the normalized

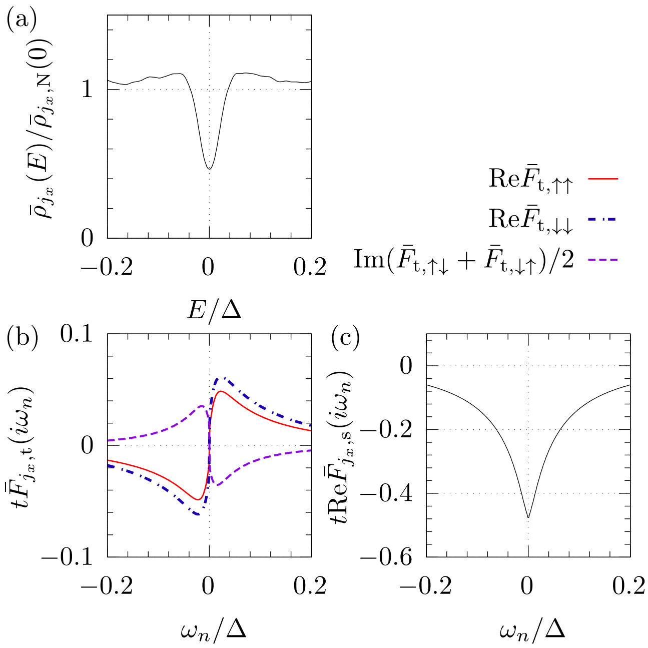

FIG. 10. (a) The normalized LDOS is plotted as a function of E. (b) $\bar{F}_{j_x,\mathrm{t}}(i\omega_n)$ is shown as a function of ω_n. (c) $\mathrm{Re}\bar{F}_{j_x,\mathrm{s}}(i\omega_n)$ is shown as a function of ω_n. $\mathrm{Im}\bar{F}_{j_x,\mathrm{t},\uparrow\uparrow}(i\omega_n) = \mathrm{Im}\bar{F}_{j_x,\mathrm{t},\downarrow\downarrow}(i\omega_n) = \mathrm{Re}[\bar{F}_{j_x,\mathrm{t},\uparrow\downarrow}(i\omega_n) + \bar{F}_{j_x,\mathrm{t},\downarrow\uparrow}(i\omega_n)] = \mathrm{Im}\bar{F}_{j_x,\mathrm{s}}(i\omega_n) = 0$ within numerical accuracy. $(\theta/2\pi, h/t) = (0.15, 0.5)$, $j_x = L_{\mathrm{NCF}} + L_{\mathrm{DN}}/2$, $L_y = 100$, and $N_{\mathrm{sample}} = 10^2$ samples averaged.

LDOS [Figs. 9(a) and 10(a)]. The spin-triplet and spin-singlet components of the anomalous Green's function are shown in Figs. 9(b), 9(c), 10(b), and 10(c). The absolute value of the spin-singlet component is larger than that of each spin-triplet component, and the spin-triplet components are linear functions at $\omega_n = 0$.

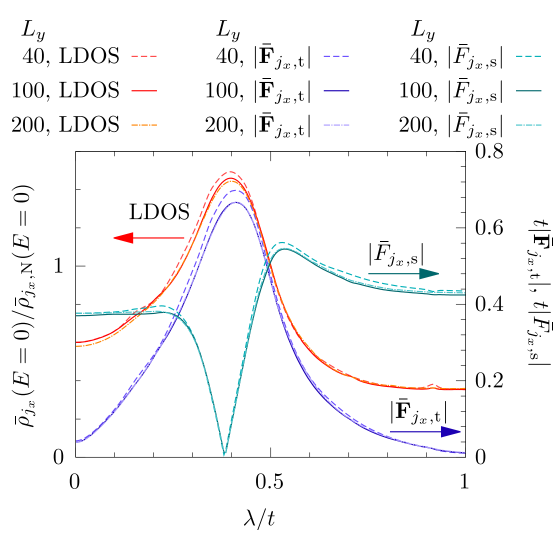

FIG. 11. The normalized zero-energy LDOS, $|\bar{\mathbf{F}}_{j_x,\mathrm{t}}(i\omega_n)|$, and $|\bar{F}_{j_x,\mathrm{s}}(i\omega_n)|$ are plotted as a function of λ with $h/t = 0.5$ and $\omega_n/t = 10^{-3}$ for several values of L_y. $j_x = L_{\mathrm{FR}} + L_{\mathrm{DN}}/2$, and $N_{\mathrm{sample}} = 10^2$ samples averaged.

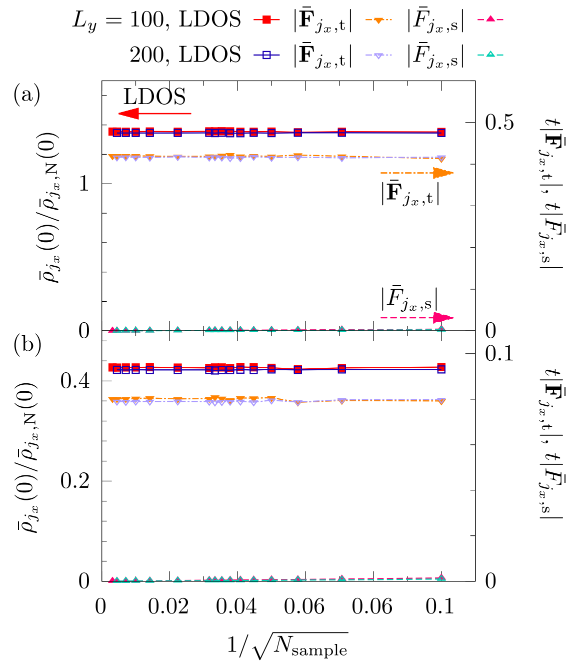

FIG. 12. The normalized zero-energy LDOS, $|\bar{\mathbf{F}}_{j_x,\mathrm{t}}(i\omega_n)|$, and $|\bar{F}_{j_x,\mathrm{s}}(i\omega_n)|$ with $\omega_n/t = 10^{-3}$ are plotted as a function of $1/\sqrt{N_{\mathrm{sample}}}$ for (a) $(\lambda/t, h/t) = (0.35, 0.5)$ and (b) (0.7,0.5). $j_x = L_{\mathrm{FR}} + L_{\mathrm{DN}}/2$ with $L_y = 100$ and 200.

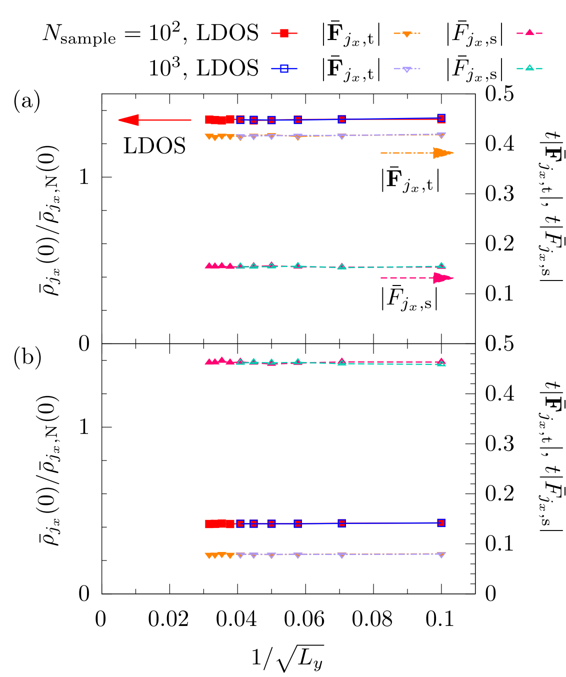

FIG. 13. The normalized zero-energy LDOS, $|\bar{\mathbf{F}}_{j_x,\mathrm{t}}(i\omega_n)|$, and $|\bar{F}_{j_x,\mathrm{s}}(i\omega_n)|$ with $\omega_n/t = 10^{-3}$ are plotted as a function of $1/\sqrt{L_y}$ for (a) $(\lambda/t, h/t) = (0.35, 0.5)$ and (b) (0.7,0.5). $j_x = L_{\mathrm{FR}} + L_{\mathrm{DN}}/2$ with $N_{\mathrm{sample}} = 10^2$ and 10^3.

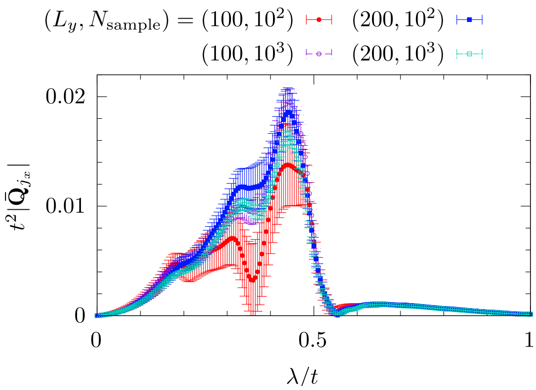

FIG. 14. $|\bar{\mathbf{Q}}_{j_x}(i\omega_n)|$ is plotted as a function of λ/t for $L_y = 100$ and 200, and $N_{\rm sample} = 10^2$ and 10^3 with $h/t = 0.5$ and $\omega_n/t = 10^{-3}$. $j_x = L_{\rm FR} + L_{\rm DN}/2$.

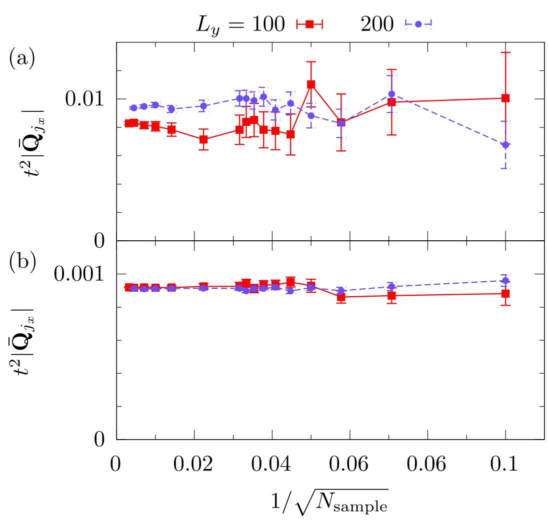

FIG. 15. $|\bar{\mathbf{Q}}_{j_x}(i\omega_n)|$ is plotted as a function of $1/\sqrt{N_{\rm sample}}$ for (a) $\lambda/t = 0.35$ and (b) 0.7 with $h/t = 0.5$ and $\omega_n/t = 10^{-3}$. $j_x = L_{\rm FR} + L_{\rm DN}/2$.

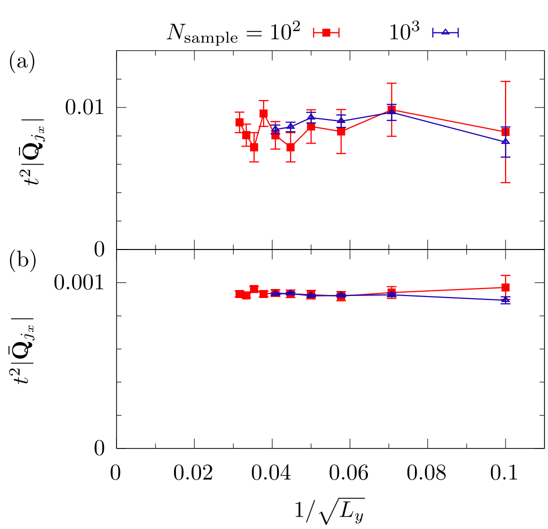

FIG. 16. $|\bar{\mathbf{Q}}_{j_x}(i\omega_n)|$ is plotted as a function of $1/\sqrt{L_y}$ for (a) $(\lambda/t, h/t) = (0.35, 0.5)$ and (b) (0.7,0.5) with $\omega_n/t = 10^{-3}$. $j_x = L_{\rm FR} + L_{\rm DN}/2$.

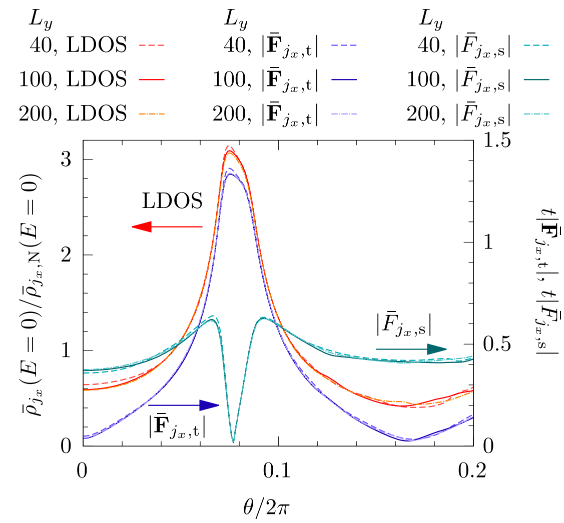

FIG. 17. The normalized LDOS, $|\bar{\mathbf{F}}_{j_x,{\rm t}}(i\omega_n)|$, and $|\bar{F}_{j_x,{\rm s}}(i\omega_n)|$ are plotted as a function of θ with $h/t = 0.5$ and $\omega_n/t = 10^{-3}$ for several values of L_y. $j_x = L_{\rm NCF} + L_{\rm DN}/2$, and $N_{\rm sample} = 10^2$ samples averaged.

APPENDIX B: SYSTEM SIZE AND SAMPLE NUMBER DEPENDENCE

Here, we show the $N_{\rm sample}$ and L_y dependences of the normalized LDOS, $|\bar{\mathbf{F}}_{j_x,{\rm t}}(i\omega_n)|$, $|\bar{F}_{j_x,{\rm s}}(i\omega_n)|$, and $|\bar{\mathbf{Q}}_{j_x}(i\omega_n)|$ in order to demonstrate the robustness of our results.

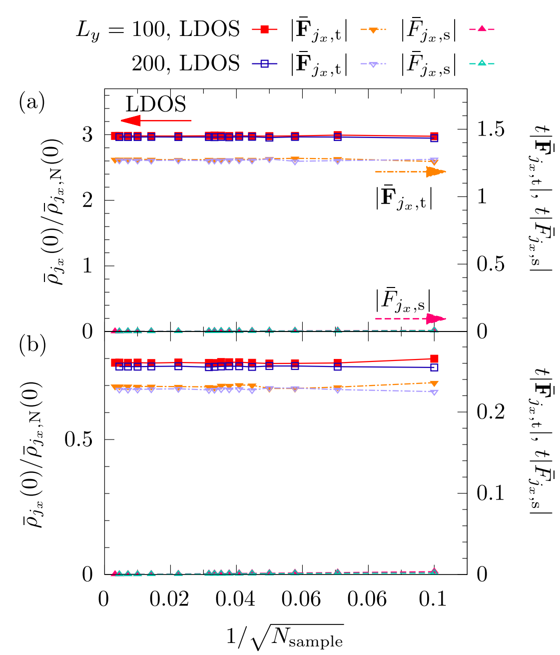

FIG. 18. The normalized zero-energy LDOS, $|\bar{\mathbf{F}}_{j_x,{\rm t}}(i\omega_n)|$, and $|\bar{F}_{j_x,{\rm s}}(i\omega_n)|$ with $\omega_n/t = 10^{-3}$ are plotted as a function of $1/\sqrt{N_{\rm sample}}$ for (a) $(\theta/2\pi, h/t) = (0.08, 0.5)$ and (b) (0.12,0.5). $j_x = L_{\rm NCF} + L_{\rm DN}/2$.

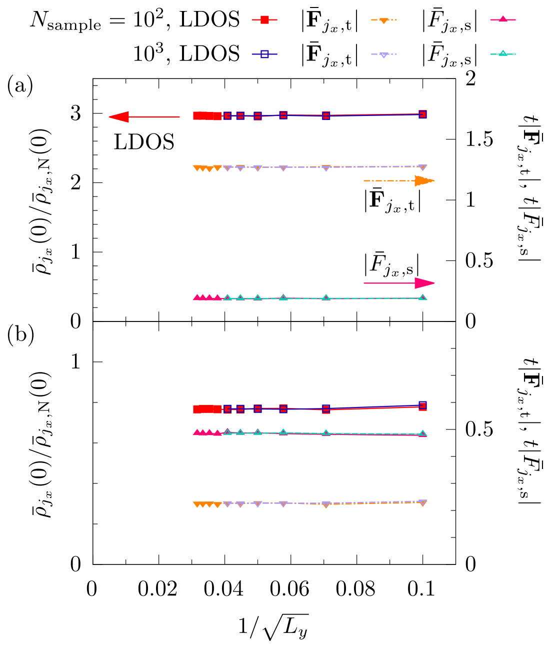

FIG. 19. The normalized zero-energy LDOS, $|\bar{\mathbf{F}}_{j_x,\text{t}}(i\omega_n)|$, and $|\bar{F}_{j_x,\text{s}}(i\omega_n)|$ with $\omega_n/t = 10^{-3}$ are plotted as a function of $1/\sqrt{L_y}$ for (a) $\theta/2\pi = 0.08$ and (b) 0.12 with $h/t = 0.5$. $j_x = L_{\text{NCF}} + L_{\text{DN}}/2$.

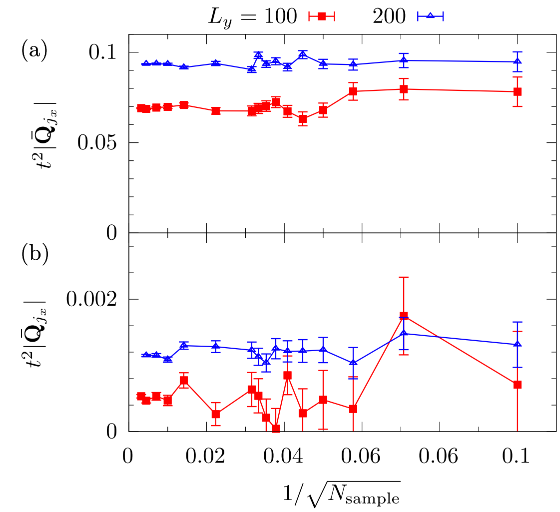

FIG. 21. $|\bar{\mathbf{Q}}_{j_x}(i\omega_n)|$ is plotted as a function of $1/\sqrt{N_{\text{sample}}}$ for (a) $\theta/2\pi = 0.08$, and (b) 0.12 with $h/t = 0.5$ and $\omega_n/t = 10^{-3}$. $j_x = L_{\text{NCF}} + L_{\text{DN}}/2$.

1. SC/FR/DN junction

We show the L_y dependences of the normalized LDOS at zero energy, $|\bar{\mathbf{F}}_{j_x,\text{t}}(i\omega_n)|$, and $|\bar{F}_{j_x,\text{s}}(i\omega_n)|$ at a low frequency in Fig. 11. Their system size dependences are not significant. In Figs. 12 and 13, we show N_{sample} and L_y dependences, respectively, at fixed λ and h. The N_{sample} and L_y dependences are also not significant in these plots.

In Fig. 14, we show $|\bar{\mathbf{Q}}_{j_x}(i\omega_n)|$ for $(L_y, N_{\text{sample}}) = (100, 10^2)$, $(100, 10^3)$, $(200, 10^2)$, and $(200, 10^3)$ at $\omega_n/t = 10^{-3}$. Here, we show the standard error as an error bar. The average values $|\bar{\mathbf{Q}}_{j_x}(i\omega_n)|$ have a large fluctuation for $0.1 \lesssim \lambda/t \lesssim 0.5$. It might correspond to the fact that the normalized LDOS at zero energy has large values close to these parameters. For $N_{\text{sample}} = 10^3$, $|\bar{\mathbf{Q}}_{j_x}(i\omega_n)|$ for $L_y = 100$ and $L_y = 200$ have almost the same value. In Fig. 15, we show the N_{sample} dependence of $|\bar{\mathbf{Q}}_{j_x}(i\omega_n)|$ for $h/t = 0.5$. $|\bar{\mathbf{Q}}_{j_x}(i\omega_n)|$ for $L_y = 100$ and 200 have almost the same value, but for large N_{sample}, $|\bar{\mathbf{Q}}_{j_x}(i\omega_n)|$ with $L_y = 100$ has a slightly smaller value at $\lambda/t = 0.35$ [Fig. 15(a)]. In Fig. 16, we show the L_y dependence of $|\bar{\mathbf{Q}}_{j_x}(i\omega_n)|$ at $h/t = 0.5$ for $N_{\text{sample}} = 10^2$ and 10^3. There are somewhat large statistical errors for $N_{\text{sample}} = 10^2$, but the size of the error bar is sufficiently small for $L_y = 100$ and $N_{\text{sample}} = 10^3$.

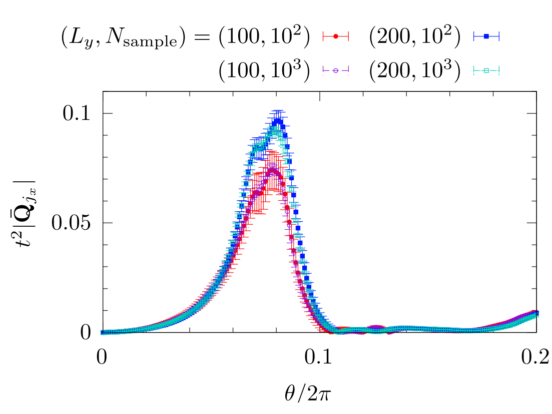

FIG. 20. $|\bar{\mathbf{Q}}_{j_x}(i\omega_n)|$ is plotted as a function of θ for several L_y and N_{sample} with $h/t = 0.5$ and $\omega_n/t = 10^{-3}$. $j_x = L_{\text{NCF}} + L_{\text{DN}}/2$.

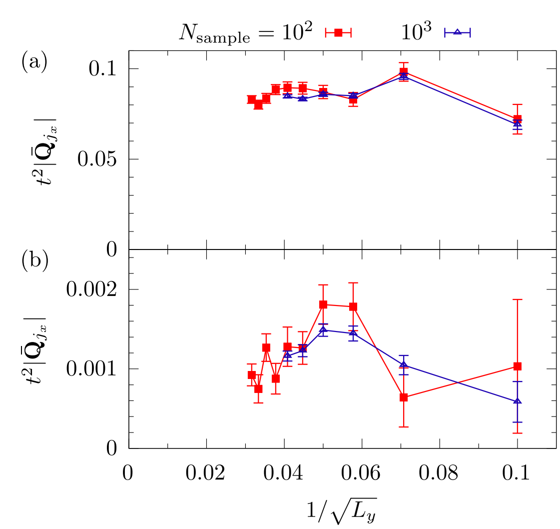

FIG. 22. $|\bar{\mathbf{Q}}_{j_x}(i\omega_n)|$ is plotted as a function of $1/\sqrt{L_y}$ for (a) $\theta/2\pi = 0.08$ and (b) 0.12 with $h/t = 0.5$ and $\omega_n/t = 10^{-3}$. $j_x = L_{\text{NCF}} + L_{\text{DN}}/2$.

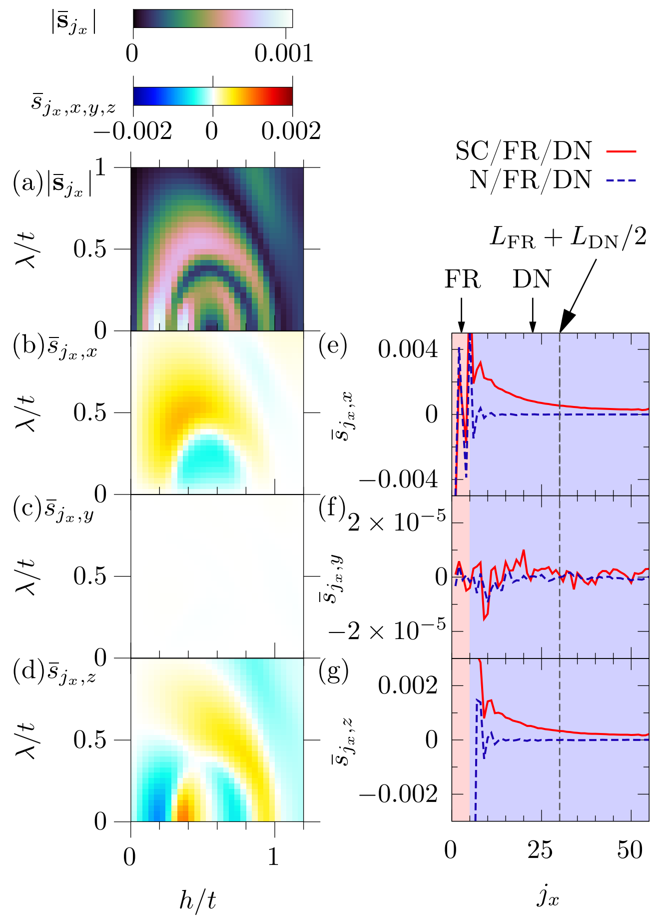

FIG. 23. (a) $|\bar{\mathbf{s}}_{j_x}|$, (b) $\bar{s}_{j_x,x}$, (c) $\bar{s}_{j_x,y}$, and (d) $\bar{s}_{j_x,z}$ are plotted as a function of h and λ at $j_x = L_{\rm FR} + L_{\rm DN}/2$. (e) $\bar{s}_{j_x,x}$, (f) $\bar{s}_{j_x,y}$, and (g) $\bar{s}_{j_x,z}$ are plotted as a function of j_x for $(\lambda/t, h/t) = (0.5, 0.5)$. $t\beta = 10^3$, $L_y = 40$, and $N_{\rm sample} = 10^2$ samples averaged.

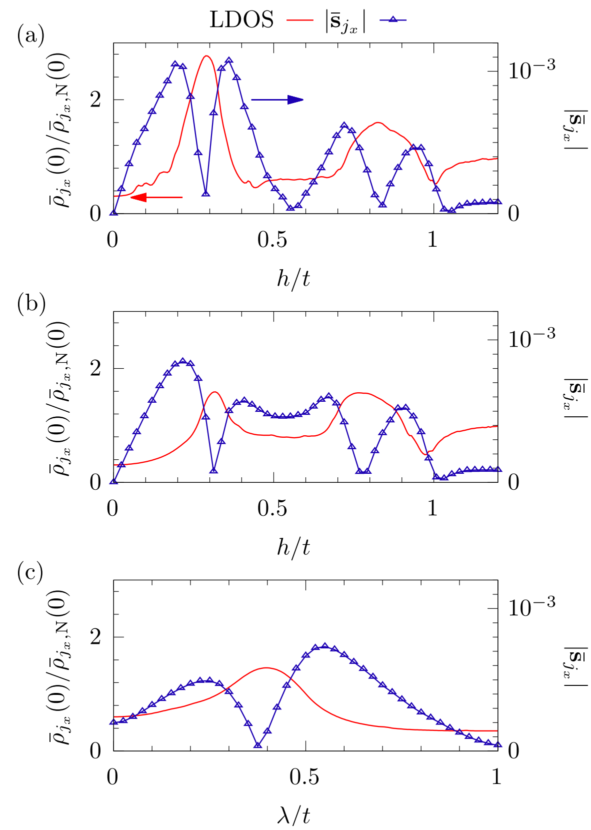

FIG. 24. The normalized zero-energy LDOS (left y axis) and $|\bar{\mathbf{s}}_{j_x}|$ (right y axis) are plotted as a function of h/t for (a) $\lambda = 0$ and (b) $\lambda/t = 0.2$ and plotted as a function of λ/t for (c) $h/t = 0.5$ at $j_x = L_{\rm FR} + L_{\rm DN}/2$. $t\beta = 10^3$, $L_y = 100$, and $N_{\rm sample} = 10^2$ samples averaged.

2. SC/NCF/DN junction

We show the $N_{\rm sample}$ and L_y dependences for the SC/NCF/DN junction. We show the L_y dependence of the normalized LDOS, $|\bar{\mathbf{F}}_{j_x,{\rm t}}(i\omega_n)|$, and $|\bar{F}_{j_x,{\rm s}}(i\omega_n)|$ at a low frequency in Fig. 17. In this case, similar to the SC/FR/DN junction, their system size dependences are weak. In Figs. 18 and 19, we show the $N_{\rm sample}$ and L_y dependences, respectively, at fixed θ and h. The $N_{\rm sample}$ and L_y dependences are also not very strong in these plots.

In Fig. 20, we show $|\bar{\mathbf{Q}}_{j_x}(i\omega_n)|$ for $(L_y, N_{\rm sample}) = (100, 10^2)$, $(100, 10^3)$, $(200, 10^2)$, and $(200, 10^3)$ at $\omega_n/t = 10^{-3}$. Here, we also show the standard error as an error bar. We also observe a large error at $0.06 \lesssim \theta/2\pi \lesssim 0.09$. $|\bar{\mathbf{Q}}_{j_x}(i\omega_n)|$ for $N_{\rm sample} = 10^2$ and 10^3 have almost the same value, but $L_y = 100$ and 200 are different for $0.06 \lesssim \theta/2\pi \lesssim 0.09$. In Fig. 21, we show the $N_{\rm sample}$ dependence of $|\bar{\mathbf{Q}}_{j_x}(i\omega_n)|$ for $h/t = 0.5$. $|\bar{\mathbf{Q}}_{j_x}(i\omega_n)|$ for $L_y = 100$ is smaller than that for 200 even for large $N_{\rm sample}$, at least for $\theta/2\pi = 0.08$ [Fig. 21(a)]. In Fig. 22, we show the L_y dependence of $|\bar{\mathbf{Q}}_{j_x}(i\omega_n)|$ at $(\theta/2\pi, h/t) = (0.08, 0.5)$ and (0.12,0,5) for $N_{\rm sample} = 10^2$ and 10^3. The L_y dependence is not small for $\theta/2\pi = 0.08$ [Fig. 22(a)], but we expect that the qualitative behaviors of the results do not change.

APPENDIX C: EXPECTATION VALUE OF SPIN OPERATOR

In this Appendix, we discuss the expectation of the spin operator:

$$\bar{s}_{j_x,\alpha} = \frac{1}{L_y N_{\rm sample}\beta} \sum_{j_y=1}^{L_y} \sum_{l=1}^{N_{\rm sample}} \sum_{n} {\rm Tr}[P\hat{\sigma}_\alpha G_{l,\mathbf{j},\mathbf{j}}(i\omega_n)], \quad \text{(C1)}$$

with $\alpha = x, y, z$ and the inverse of the temperature β. Here, we use an IR basis to calculate the Matsubara frequency sum [78], which reduces the computational cost. In the following, we choose $\beta t = 10^3$. We confirmed that the results are almost the same as the results with $\beta t = 10^4$, and thus, $\beta t = 10^3$ is a sufficiently small temperature.

1. SC/FR/DN junction

In Fig. 23, we show the expectation value of the spin operator [Figs. 23(a)–23(d)] and its spatial dependence [Figs. 23(e)–23(g)] for the SC/FR/DN junction. $|\bar{\mathbf{s}}_{j_x}|$ has a small value in the region where the normalized LDOS at zero energy exceeds unity and has a large value [Fig. 3(a); see also Fig. 24]. This might be understood as follows: the LDOS at zero energy might have a maximum when both the spin-up and -down components of the LDOS have large values, and

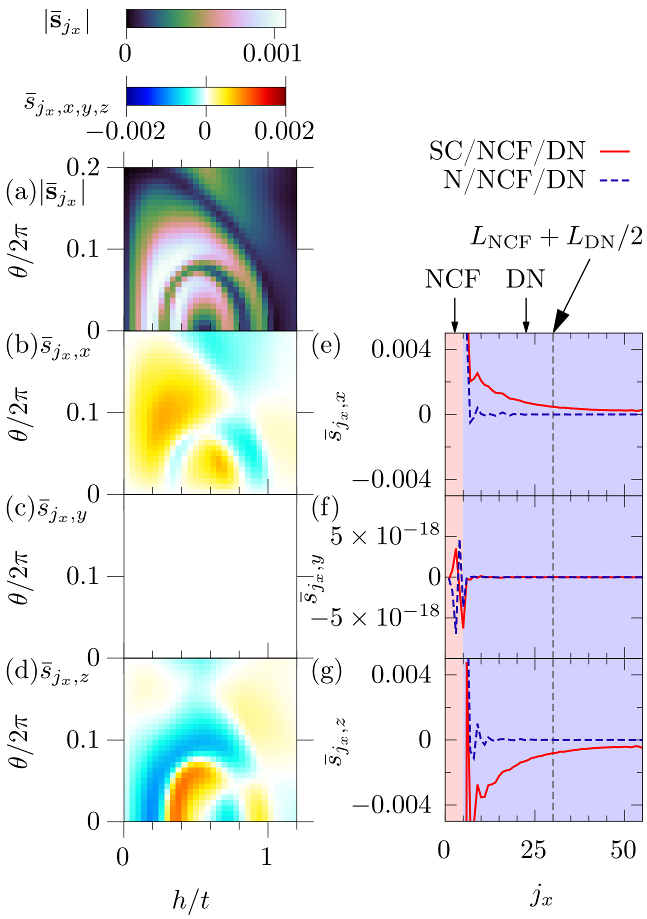

FIG. 25. (a) $|\bar{\mathbf{s}}_{j_x}|$, (b) $\bar{s}_{j_x,x}$, (c) $\bar{s}_{j_x,y}$, and (d) $\bar{s}_{j_x,z}$ are plotted as a function of h and θ at $j_x = L_{\rm NCF} + L_{\rm DN}/2$. (e) $\bar{s}_{j_x,x}$, (f) $\bar{s}_{j_x,y}$, and (g) $\bar{s}_{j_x,z}$ are plotted as a function of j_x for $(h/t, \theta/2\pi) = (0.5, 0.1)$. $t\beta = 10^3$, $L_y = 40$, and $N_{\rm sample} = 10^2$ samples averaged.

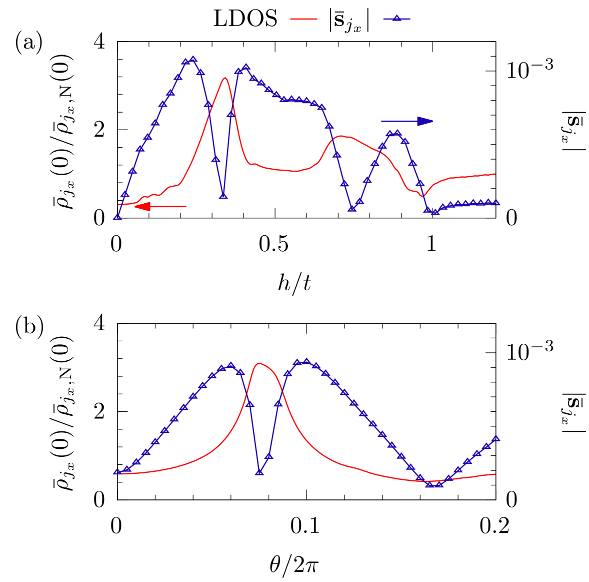

FIG. 26. The normalized zero-energy LDOS (left y axis) and $|\bar{\mathbf{s}}_{j_x}|$ (right y axis) are plotted as a function of (a) h/t for $\theta/2\pi = 0.05$ and (b) $\theta/2\pi$ for $h/t = 0.5$ at $j_x = L_{\rm NCF} + L_{\rm DN}/2$. $t\beta = 10^3$, $L_y = 100$, and $N_{\rm sample} = 10^2$ samples averaged.

as a consequence, the expectation value of the spin becomes small (minimum) in the DN.

$|\bar{\mathbf{s}}_{j_x}|$ becomes nonzero at $\lambda = 0$ in some region where the polarized spin-triplet Cooper pair amplitude is zero. In general, both the quasiparticles and the Cooper pairs contribute to $\bar{\mathbf{s}}_{j_x}$. Thus, the nonzero value of $\bar{\mathbf{s}}_{j_x}$ at $\lambda = 0$ comes from spin polarization of the quasiparticles. Therefore, the nonzero value of $\bar{\mathbf{s}}_{j_x}$ is not direct evidence of the presence of the polarized spin-triplet Cooper pair amplitude. $\bar{\mathbf{s}}_{j_x}$ has only x and z components, similar to $\bar{\mathbf{Q}}_{j_x}(i\omega_n)$ in Figs. 5(b)–5(d). In Figs. 23(e)–23(g), we show the spatial dependence of $\bar{\mathbf{s}}_{j_x}$ for the SC/FR/DN and N/FR/DN junctions (for N, we set the pair potential $\Delta = 0$, and the other parameters are the same as in the corresponding SC junctions). We can see that the presence of the SC is crucial for the nonzero value of $\bar{s}_{j_x,x}$, and $\bar{s}_{j_x,z}$ in the DN.

2. SC/NCF/DN junction

We can see similar behaviors for the SC/NCF/DN junction (Figs. 25 and 26). In this case, $|\bar{\mathbf{s}}_{j_x}|$ also becomes small in the region where the normalized LDOS at zero energy exceeds unity [Figs. 25(a) and 26]. Also, $\bar{\mathbf{s}}_{j_x}$ penetrates the DN due to the superconducting proximity effect [Figs. 25(e)–25(g)].

[1] A. I. Buzdin, Proximity effects in superconductor-ferromagnet heterostructures, Rev. Mod. Phys. **77**, 935 (2005).

[2] F. S. Bergeret, A. F. Volkov, and K. B. Efetov, Odd triplet superconductivity and related phenomena in superconductor-ferromagnet structures, Rev. Mod. Phys. **77**, 1321 (2005).

[3] M. Eschrig, Spin-polarized supercurrents for spintronics, Phys. Today **64**(1), 43 (2011).

[4] J. Linder and J. W. A. Robinson, Superconducting spintronics, Nat. Phys. **11**, 307 (2015).

[5] F. S. Bergeret, A. F. Volkov, and K. B. Efetov, Long-Range Proximity Effects in Superconductor-Ferromagnet Structures, Phys. Rev. Lett. **86**, 4096 (2001).

[6] F. S. Bergeret, A. F. Volkov, and K. B. Efetov, Josephson current in superconductor-ferromagnet structures with a nonhomogeneous magnetization, Phys. Rev. B **64**, 134506 (2001).

[7] R. S. Keizer, S. T. B. Goennenwein, T. M. Klapwijk, G. Miao, G. Xiao, and A. Gupta, A spin triplet supercurrent through the half-metallic ferromagnet CrO_2, Nature (London) **439**, 825 (2006).

[8] T. S. Khaire, M. A. Khasawneh, W. P. Pratt, and N. O. Birge, Observation of Spin-Triplet Superconductivity in Co-Based Josephson Junctions, Phys. Rev. Lett. **104**, 137002 (2010).

[9] J. W. A. Robinson, J. D. S. Witt, and M. G. Blamire, Controlled Injection of Spin-Triplet Supercurrents into a Strong Ferromagnet, Science **329**, 59 (2010).

[10] M. Eschrig, Spin-polarized supercurrents for spintronics: A review of current progress, Rep. Prog. Phys. **78**, 104501 (2015).

[11] X. Waintal and P. W. Brouwer, Magnetic exchange interaction induced by a Josephson current, Phys. Rev. B **65**, 054407 (2002).

[12] J. Linder and T. Yokoyama, Supercurrent-induced magnetization dynamics in a Josephson junction with two misaligned ferromagnetic layers, Phys. Rev. B **83**, 012501 (2011).

[13] I. Kulagina and J. Linder, Spin supercurrent, magnetization dynamics, and φ-state in spin-textured Josephson junctions, Phys. Rev. B **90**, 054504 (2014).

[14] I. V. Bobkova, A. M. Bobkov, and M. A. Silaev, Spin torques and magnetic texture dynamics driven by the supercurrent in superconductor/ferromagnet structures, Phys. Rev. B **98**, 014521 (2018).

[15] R. Takashima, S. Fujimoto, and T. Yokoyama, Adiabatic and nonadiabatic spin torques induced by a spin-triplet supercurrent, Phys. Rev. B **96**, 121203(R) (2017).

[16] F. S. Bergeret and I. V. Tokatly, Singlet-Triplet Conversion and the Long-Range Proximity Effect in Superconductor-Ferromagnet Structures with Generic Spin Dependent Fields, Phys. Rev. Lett. **110**, 117003 (2013).

[17] F. S. Bergeret and I. V. Tokatly, Spin-orbit coupling as a source of long-range triplet proximity effect in superconductor-ferromagnet hybrid structures, Phys. Rev. B **89**, 134517 (2014).

[18] M. A. Silaev, I. V. Tokatly, and F. S. Bergeret, Anomalous current in diffusive ferromagnetic Josephson junctions, Phys. Rev. B **95**, 184508 (2017).

[19] M. A. Silaev, I. V. Bobkova, and A. M. Bobkov, Odd triplet superconductivity induced by a moving condensate, Phys. Rev. B **102**, 100507(R) (2020).

[20] S. H. Jacobsen, J. A. Ouassou, and J. Linder, Critical temperature and tunneling spectroscopy of superconductor-ferromagnet hybrids with intrinsic Rashba-Dresselhaus spin-orbit coupling, Phys. Rev. B **92**, 024510 (2015).

[21] P. Burset, B. Lu, G. Tkachov, Y. Tanaka, E. M. Hankiewicz, and B. Trauzettel, Superconducting proximity effect in three-dimensional topological insulators in the presence of a magnetic field, Phys. Rev. B **92**, 205424 (2015).

[22] A. Buzdin, Direct Coupling Between Magnetism and Superconducting Current in the Josephson φ_0 Junction, Phys. Rev. Lett. **101**, 107005 (2008).

[23] F. Konschelle, I. V. Tokatly, and F. S. Bergeret, Theory of the spin-galvanic effect and the anomalous phase shift φ_0 in superconductors and Josephson junctions with intrinsic spin-orbit coupling, Phys. Rev. B **92**, 125443 (2015).

[24] Y. Tanaka, T. Yokoyama, and N. Nagaosa, Manipulation of the Majorana Fermion, Andreev Reflection, and Josephson Current on Topological Insulators, Phys. Rev. Lett. **103**, 107002 (2009).

[25] I. V. Tokatly, Usadel equation in the presence of intrinsic spin-orbit coupling: A unified theory of magnetoelectric effects in normal and superconducting systems, Phys. Rev. B **96**, 060502(R) (2017).

[26] I. Bobkova, A. Bobkov, and M. Silaev, Magnetoelectric effects in Josephson junctions, J. Phys.: Condens. Matter **34**, 353001 (2022).

[27] K.-R. Jeon, C. Ciccarelli, A. J. Ferguson, H. Kurebayashi, L. F. Cohen, X. Montiel, M. Eschrig, J. W. A. Robinson, and M. G. Blamire, Enhanced spin pumping into superconductors provides evidence for superconducting pure spin currents, Nat. Mater. **17**, 499 (2018).

[28] J. Linder, T. Yokoyama, A. Sudbø, and M. Eschrig, Pairing Symmetry Conversion by Spin-Active Interfaces in Magnetic Normal-Metal–Superconductor Junctions, Phys. Rev. Lett. **102**, 107008 (2009).

[29] J. Linder, A. Sudbø, T. Yokoyama, R. Grein, and M. Eschrig, Signature of odd-frequency pairing correlations induced by a magnetic interface, Phys. Rev. B **81**, 214504 (2010).

[30] S. Pal and C. Benjamin, Exciting odd-frequency equal-spin triplet correlations at metal-superconductor interfaces, Phys. Rev. B **104**, 054519 (2021).

[31] E. Strambini, V. N. Golovach, G. De Simoni, J. S. Moodera, F. S. Bergeret, and F. Giazotto, Revealing the magnetic proximity effect in EuS/Al bilayers through superconducting tunneling spectroscopy, Phys. Rev. Mater. **1**, 054402 (2017).

[32] M. Rouco, S. Chakraborty, F. Aikebaier, V. N. Golovach, E. Strambini, J. S. Moodera, F. Giazotto, T. T. Heikkilä, and F. S. Bergeret, Charge transport through spin-polarized tunnel junction between two spin-split superconductors, Phys. Rev. B **100**, 184501 (2019).

[33] A. Hijano, S. Ilić, M. Rouco, C. González-Orellana, M. Ilyn, C. Rogero, P. Virtanen, T. T. Heikkilä, S. Khorshidian, M. Spies, N. Ligato, F. Giazotto, E. Strambini, and F. S. Bergeret, Coexistence of superconductivity and spin-splitting fields in superconductor/ferromagnetic insulator bilayers of arbitrary thickness, Phys. Rev. Res. **3**, 023131 (2021).

[34] A. Pal, J. A. Ouassou, M. Eschrig, J. Linder, and M. G. Blamire, Spectroscopic evidence of odd frequency superconducting order, Sci. Rep. **7**, 40604 (2017).

[35] S. Diesch, P. Machon, M. Wolz, C. Sürgers, D. Beckmann, W. Belzig, and E. Scheer, Creation of equal-spin triplet superconductivity at the Al/EuS interface, Nat. Commun. **9**, 5248 (2018).

[36] Y. Asano, Y. Tanaka, and A. A. Golubov, Josephson Effect due to Odd-Frequency Pairs in Diffusive Half Metals, Phys. Rev. Lett. **98**, 107002 (2007).

[37] V. Braude and Y. V. Nazarov, Fully Developed Triplet Proximity Effect, Phys. Rev. Lett. **98**, 077003 (2007).

[38] T. Yokoyama, Y. Tanaka, and A. A. Golubov, Manifestation of the odd-frequency spin-triplet pairing state in diffusive ferromagnet/superconductor junctions, Phys. Rev. B **75**, 134510 (2007).

[39] Y. Tanaka and A. A. Golubov, Theory of the Proximity Effect in Junctions with Unconventional Superconductors, Phys. Rev. Lett. **98**, 037003 (2007).

[40] Y. Tanaka, M. Sato, and N. Nagaosa, Symmetry and Topology in Superconductors, -Odd-Frequency Pairing and Edge States-, J. Phys. Soc. Jpn. **81**, 011013 (2012).

[41] L. G. Johnsen, H. T. Simensen, A. Brataas, and J. Linder, Magnon Spin Current Induced by Triplet Cooper Pair Supercurrents, Phys. Rev. Lett. **127**, 207001 (2021).

[42] I. V. Bobkova, A. M. Bobkov, A. Kamra, and W. Belzig, Magnon-cooparons in magnet-superconductor hybrids, Commun. Mater. **3**, 95 (2022).

[43] A. Hijano, V. N. Golovach, and F. S. Bergeret, Quasiparticle density of states and triplet correlations in superconductor/ferromagnetic-insulator structures across a sharp domain wall, Phys. Rev. B **105**, 174507 (2022).

[44] S. Tamura and Y. Tanaka, Theory of the proximity effect in two-dimensional unconventional superconductors with Rashba spin-orbit interaction, Phys. Rev. B **99**, 184501 (2019).

[45] Y. Asano and Y. Tanaka, Majorana fermions and odd-frequency Cooper pairs in a normal-metal nanowire proximity-coupled to a topological superconductor, Phys. Rev. B **87**, 104513 (2013).

[46] Here, we consider a ballistic barrier because an insulating barrier greatly suppresses the amplitude of Cooper pair in the DN.

[47] A. Umerski, Closed-form solutions to surface Green's functions, Phys. Rev. B **55**, 5266 (1997).

[48] V. L. Berezinskii, New model of the anisotropic phase of superfluid He^3, Pis'ma Zh. Eksp. Teor. Fiz. **20**, 628 (1974) [JETP Lett. **20** 287 (1974)].

[49] J. Linder and A. V. Balatsky, Odd-frequency superconductivity, Rev. Mod. Phys. **91**, 045005 (2019).

[50] J. Cayao, C. Triola, and A. M. Black-Schaffer, Odd-frequency superconducting pairing in one-dimensional systems, Eur. Phys. J.: Spec. Top. **229**, 545 (2020).

[51] W. Belzig, C. Bruder, and G. Schön, Local density of states in a dirty normal metal connected to a superconductor, Phys. Rev. B **54**, 9443 (1996).

[52] Y. Tanaka, A. A. Golubov, and S. Kashiwaya, Theory of charge transport in diffusive normal metal/conventional superconductor point contacts, Phys. Rev. B **68**, 054513 (2003).

[53] Y. Tanaka, A. A. Golubov, S. Kashiwaya, and M. Ueda, Anomalous Josephson Effect between Even- and Odd-Frequency Superconductors, Phys. Rev. Lett. **99**, 037005 (2007).

[54] Y. Tanaka, Y. Tanuma, and A. A. Golubov, Odd-frequency pairing in normal-metal/superconductor junctions, Phys. Rev. B **76**, 054522 (2007).

[55] A. J. Leggett, A theoretical description of the new phases of liquid ^{3}He, Rev. Mod. Phys. **47**, 331 (1975).

[56] M. Alidoust, J. Linder, G. Rashedi, T. Yokoyama, and A. Sudbø, Spin-polarized Josephson current in superconductor/ferromagnet/superconductor junctions with inhomogeneous magnetization, Phys. Rev. B **81**, 014512 (2010).

[57] T. Champel and M. Eschrig, Switching superconductivity in superconductor/ferromagnet bilayers by multiple-domain structures, Phys. Rev. B **71**, 220506(R) (2005).

[58] T. Champel and M. Eschrig, Effect of an inhomogeneous exchange field on the proximity effect in disordered superconductor-ferromagnet hybrid structures, Phys. Rev. B **72**, 054523 (2005).

[59] N. Kanazawa, S. Seki, and Y. Tokura, Noncentrosymmetric magnets hosting magnetic skyrmions, Adv. Mater. **29**, 1603227 (2017).

[60] Y. Fujishiro, N. Kanazawa, and Y. Tokura, Engineering skyrmions and emergent monopoles in topological spin crystals, Appl. Phys. Lett. **116**, 090501 (2020).

[61] C. Pappas, E. Lelièvre-Berna, P. Falus, P. M. Bentley, E. Moskvin, S. Grigoriev, P. Fouquet, and B. Farago, Chiral Paramagnetic Skyrmion-Like Phase in MnSi, Phys. Rev. Lett. **102**, 197202 (2009).

[62] N. Kanazawa, Y. Onose, T. Arima, D. Okuyama, K. Ohoyama, S. Wakimoto, K. Kakurai, S. Ishiwata, and Y. Tokura, Large Topological Hall Effect in a Short-Period Helimagnet MnGe, Phys. Rev. Lett. **106**, 156603 (2011).

[63] E. Vélez-Fort *et al.*, Ferromagnetism and Rashba spin–orbit coupling in the two-dimensional (V, Pt)Se_2 alloy, ACS Appl. Electron. Mater. **4**, 259 (2022).

[64] M. Matsuda, D. Zhang, Y. Kuwata, Q. Zhang, T. Sakurai, H. Ohta, H. Sugawara, K. Takeda, J. Hayashi, and H. Kotegawa, Noncollinear spin structure with weak ferromagnetism in NbMnP, Phys. Rev. B **104**, 174413 (2021).

[65] C.-R. Hu, Midgap Surface States as a Novel Signature for d^2_{xa}-x^2_b-wave superconductivity, Phys. Rev. Lett. **72**, 1526 (1994).

[66] Y. Tanaka and S. Kashiwaya, Theory of Tunneling Spectroscopy of d-Wave Superconductors, Phys. Rev. Lett. **74**, 3451 (1995).

[67] S. Kashiwaya and Y. Tanaka, Tunnelling effects on surface bound states in unconventional superconductors, Rep. Prog. Phys. **63**, 1641 (2000).

[68] S. Tamura, S. Hoshino, and Y. Tanaka, Odd-frequency pairs in chiral symmetric systems: Spectral bulk-boundary correspondence and topological criticality, Phys. Rev. B **99**, 184512 (2019).

[69] S.-P. Lee, R. M. Lutchyn, and J. Maciejko, Odd-frequency superconductivity in a nanowire coupled to Majorana zero modes, Phys. Rev. B **95**, 184506 (2017).

[70] J. Cayao and A. M. Black-Schaffer, Odd-frequency superconducting pairing in junctions with Rashba spin-orbit coupling, Phys. Rev. B **98**, 075425 (2018).

[71] T. Yokoyama, Josephson and proximity effects on the surface of a topological insulator, Phys. Rev. B **86**, 075410 (2012).

[72] A. M. Black-Schaffer and A. V. Balatsky, Odd-frequency superconducting pairing in topological insulators, Phys. Rev. B **86**, 144506 (2012).

[73] A. M. Black-Schaffer and A. V. Balatsky, Proximity-induced unconventional superconductivity in topological insulators, Phys. Rev. B **87**, 220506(R) (2013).

[74] F. Crépin, P. Burset, and B. Trauzettel, Odd-frequency triplet superconductivity at the helical edge of a topological insulator, Phys. Rev. B **92**, 100507(R) (2015).

[75] A. S. Vasenko, A. A. Golubov, V. M. Silkin, and E. V. Chulkov, Odd-frequency superconductivity induced in topological insulators with and without hexagonal warping, J. Phys.: Condens. Matter **29**, 295502 (2017).

[76] J. Cayao and A. M. Black-Schaffer, Odd-frequency superconducting pairing and subgap density of states at the edge of a two-dimensional topological insulator without magnetism, Phys. Rev. B **96**, 155426 (2017).

[77] J. A. Krieger, A. Pertsova, S. R. Giblin, M. Döbeli, T. Prokscha, C. W. Schneider, A. Suter, T. Hesjedal, A. V. Balatsky, and Z. Salman, Proximity-Induced Odd-Frequency Superconductivity in a Topological Insulator, Phys. Rev. Lett. **125**, 026802 (2020).

[78] N. Chikano, K. Yoshimi, J. Otsuki, and H. Shinaoka, Irbasis: Open-source database and software for intermediate-representation basis functions of imaginary-time Green's function, Comput. Phys. Commun. **240**, 181 (2019).